POWER EVALUATION FOR FLUTTER-BASED ELECTROMAGNETIC ENERGY HARVESTER USING CFD SIMULATIONS

J. Park[1], G. Morgenthal[2], K. Kim[3], S. Kwon[3], and Kincho Law[1]

Abstract: Structural instability caused by self exciting aerodynamic forces (flutter) can be used as an effective input source for small scale energy harvesters. The self exciting aerodynamic force exerted on a T-shape cantilever causes periodic vibration, which can be converted into electric power through an electromagnetic transducer. Due to the complexities inherent in the fluid-structure interaction between the cantilever harvester and wind flow, analyzing the structural response of the cantilever and estimating the power output from the flutter based energy harvester is challenging. Here, a CFD code based on the Vortex Particle Method is employed to simulate the wind induced responses of a T-shape cantilever beam and to estimate the power output extracted from the flutter vibration. The estimated aerodynamic damping parameter, together with the mechanical and electrical damping parameters in the harvester are then used to find the critical wind speed of flutter onset as well as the optimum load resistance. Results are supported by wind tunnel tests conducted.

1. INTRODUCTION

Energy harvesting has been an active research area as demands for renewable energy sources increase. Energy harvesting systems refer to devices that capture and transform energy from the environment into electricity. Unlike conventional, large-scale renewable energy

[1] Department of Civil and Environmental Engineering, Stanford University, Stanford, CA, USA
[2] Institute for Structural Engineering, Bauhaus University, Weimar, Germany
[3] KOCED Wind Tunnel Center, Department of Civil Engineering, Chonbuk National University, Chonju, Korea

generating systems such as wind turbines, thermal generators, and solar panels, energy harvesting devices mostly target for powering small electronic devices. For example, many researchers are investigating how to supply power to wireless sensor modules using energy harvesters (Roundy and Wright, 2004). If such sensors can be operated solely on power generated from an energy harvester, the need to change batteries regularly can be eliminated and the maintenance cost of wireless sensor networks can be reduced.

Wind energy has long been used to generate power mostly using wind turbines by exploiting the blades' lift and drag forces to rotate an electromagnetic generator. This conventional approach for generating power is, however, difficult to apply to small scale energy harvesters, because small size generators are difficult to fabricate and have low efficiency. Wind induced vibrations have been suggested as an alternate input source for small scale energy harvesters. Such vibrations have been used to mechanically strain piezoelectric transducers to generate power (Allen and Smith, 2001; Sun et al., 2011) and to generate inductance power in electromagnetic transducers (Jung, Kim and Jang, 2011). An aero-elastic instability phenomenon such as flutter has also been proposed as an input source for energy harvesters. Flutter vibration of a T-shape cantilever beam and plate have been used to mechanically strain piezoelectric patches to generate power (Kwon, 2010; Bryant, Wolff and Garcia, 2011). A leaf-like structure has also been proposed to convert cross-flow flutter into electricity using Poly Vinylidene Fluoride (Li, Yuan and Lipson, 2011).

Flutter is a phenomenon that engineers have strived to prevent since aeroelastic instability of air plane wings or bridge girders can lead to destructive structural failure. In bridge engineering in particular researchers have conducted myriad wind tunnel tests to understand the flutter phenomenon using scaled structural models. With advancements in computing power, Computational Fluid Dynamics (CFD) has also been used and contributed significantly to understanding aerodynamic phenomena (Morgental et al., 2012) and

designing aerodynamically stable bridge sections (Larsen, 1998). In this paper, on the contrary, we seek to design aerodynamically unstable shapes to invoke the flutter induced vibration and to use it as an input source for the electromagnetic energy harvester. A CFD code based on the Vortex Particle Method (Morgental, 2007) is used to analyze the vibrational responses and the power output from the energy harvester under different wind speeds and electrical load resistances.
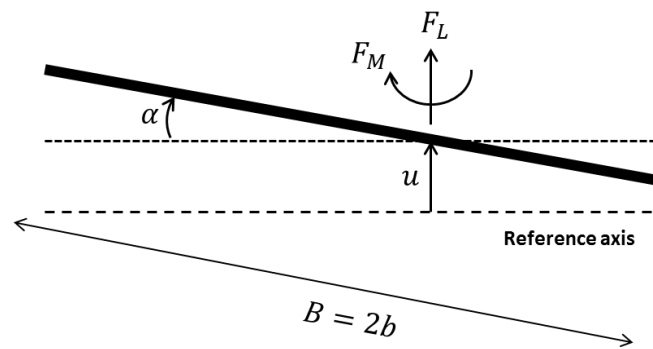

Figure 1: Coupled bending and rotational motions in the plate.

2. THEORETICAL BACKGROUND

2.1 Analytical descriptions for flutter

Flutter is a well-known dynamic excitation phenomenon in wind engineering, e.g. of bridges, where a structure becomes aerodynamically unstable through a coupled motion in the vertical bending and the torsional direction as shown in Figure 1. The corresponding equations of motion for the two degrees of freedom can be written as:

$$m\ddot{h} + 2m\zeta_h\omega_h\dot{h} + m\omega_h^2 h = F_L(t) \tag{1}$$

$$M_\alpha\ddot{\alpha} + 2M_\alpha\zeta_\alpha\omega_\alpha\dot{\alpha} + M_\alpha\omega_\alpha^2\alpha = F_M(t) \tag{2}$$

where m and M_α are, respectively, the mass and the moment of inertia (rotational mass); ζ_h and ζ_α are, respectively, the damping ratios in bending and torsional modes; h and α are, respectively, the deflection and the rotation; and ω_h and ω_α are, respectively, the natural circular frequencies for the bending and torsional modes. The motion-induced aerodynamic lift force $F_L(t)$ and moment $F_M(t)$ can be expressed through the well-known aerodynamic derivatives as (Scanlan and Tomko, 1971):

$$F_L(t) = \frac{1}{2}\rho U_\infty^2 B \left[KH_1^*(K)\frac{\dot{h}}{U_\infty} + KH_2^*(K)\frac{B\dot{\alpha}}{U_\infty} + K^2 H_3^*(K)\alpha + K^2 H_4^*(K)\frac{h}{B} \right], \quad K = \frac{\omega_h B}{U_\infty} \quad (3)$$

$$F_M(t) = \frac{1}{2}\rho U_\infty^2 B^2 \left[KA_1^*(K)\frac{\dot{h}}{U_\infty} + KA_2^*(K)\frac{B\dot{\alpha}}{U_\infty} + K^2 A_3^*(K)\alpha + K^2 A_4^*(K)\frac{h}{B} \right], \quad K = \frac{\omega_\alpha B}{U_\infty} \quad (4)$$

where ρ, U_∞ and B are, respectively, the air density, the free stream wind speed, and the section length. H_1^*, H_2^*, H_3^* and H_4^* are the flutter derivatives for the vertical force and A_1^*, A_2^*, A_3^* and A_4^* are the flutter derivatives for the rotational torsion. Furthermore, K is the non-dimensional reduced frequency.

Through the set of derivatives, the motion-induced forces are expressed as a linear combination of the instantaneous displacements and velocities of the motion. Substituting Eq. (4) into Eq. (2) and neglecting the bending mode leads to the following second order differential equation representing a simple 1-DOF, free vibration problem:

$$M_\alpha \ddot{\alpha} + \left\{ 2M_\alpha \zeta_m \omega_\alpha - \frac{1}{2}\rho U_\infty B^3 KA_2^*(K) \right\}\dot{\alpha} + \left\{ M_\alpha \omega_\alpha^2 - \frac{1}{2}\rho U_\infty^2 B^2 K^2 A_3^*(K) \right\}\alpha = 0 \quad (5)$$

The term ζ_a is replaced with ζ_m to indicate that the rotational damping is intrinsically induced by the mechanical system. The terms $2M_\alpha\zeta_m\omega_\alpha$ and $-1/2\rho U_\infty B^3 K A_2^*(K)$ are, respectively, the mechanical and the aerodynamic damping in the torsional mode. The system damping (sum of the mechanical and aerodynamic damping) and the stiffness are affected by the flutter derivatives whose values are highly dependent on the geometry of the cantilever section and the wind speed. An analytical expression for the motion-induced forces of thin plates in terms of the flutter derivatives (Scanlan and Tomko, 1971) is due to Theodorsen (1935). The flutter derivatives of an arbitrary section can be determined physically, for example, by wind tunnel tests. Furthermore, CFD simulations can be used to find the flutter derivatives for sections with a complex geometry.

2.2 Electromagnetic (EM) transducer

Energy harvesters using an electromagnetic transducer are usually built using an inertial frame configuration in which the relative movement between the magnet and the coil is induced by the vibration of the inertial frame. Instead of the inertial frame vibration, in this paper, wind flow is used as an input source for inducing the relative movement between the coil and the magnet. In particular, the wind induced flutter is utilized to convert wind flow energy into the mechanical vibrational energy. The mechanical vibrational energy then is converted into the electrical power through the electromagnetic transducer as shown in Figure 2.

Coil (R_C, N, l)

Load resistance (R_L)
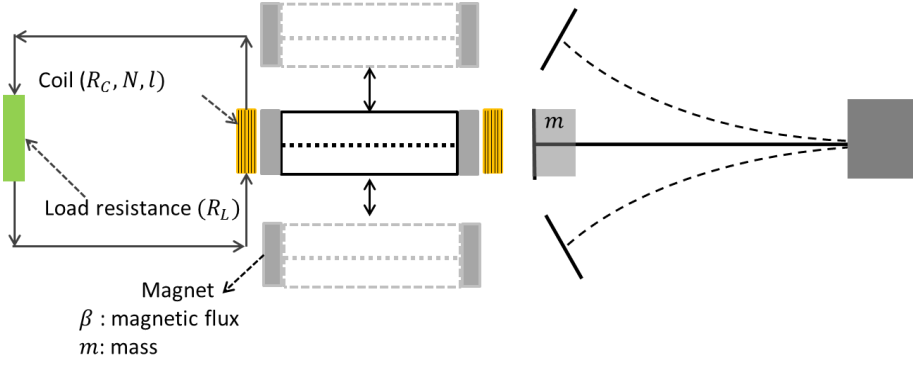
m

Magnet

β : magnetic flux

m: mass

Figure 2: Electromagnetic transducer utilizing flutter induced

The motion of the flutter based energy harvester section can be described as a forced vibration equation as follows (Beeby et al., 2007):

$$m\ddot{z}(t) + c_t \dot{z}(t) + kz(t) = F_{wind}(t) \tag{6}$$

where m, c_t and k are, respectively, the mass, total damping and stiffness of the vibration frame; z denotes the relative displacement between the magnet and the coil; and $F_{wind}(t)$ is the motion induced force corresponding to wind flow. Eq. (6) will be approximated in terms of a rigid body rotational motion, as will be discussed in a later section. The total damping coefficient (of the harvester) c_t includes both the mechanical and the electrical damping (i.e., $c_t = c_m + c_e$). The mechanical damping ($c_m = 2m\zeta_m\omega_n$) is expressed in terms of the mass m, mechanical damping ratio ζ_m and the natural frequency ω_n. The electrical damping c_e is expressed as (El-hami et al., 2001):

$$c_e = \frac{\left(Nl\beta\right)^2}{R_L + R_C + j\omega L_C} \tag{7}$$

where N, l and β are, respectively, the number of coil turns, the coil length exposed to the magnetic flux and the average flux density. Furthermore, R_L, R_C and L_C are, respectively, the load resistance, the coil resistance and the coil inductance; and ω is the angular frequency in the motion between the magnet and the coil. The coil inductance is generally negligible.

The generated energy is equivalent to the energy extracted by the electrical damping from the system as:

$$P = c_e \dot{z}^2 \tag{8}$$

where $\dot{z}$ is the relative speed between the magnet and the coil. Note that $\dot{z}$ is itself a function of electrical damping c_e since the total damping c_t including c_e suppresses the displacement z. That is, power generation depends on both the electrical and structural parameters.

2.3 Aerodynamic instability analysis based on CFD

Computational Fluid Dynamics (CFD) has been employed to evaluate the aerodynamic instability of bridge sections. For example, a Vortex Particle Method (VPM) implementation has been used for evaluating aerodynamic stability of different bridge sections (Larsen and Walther, 1998). VXflow, the VPM code employed in this study, has been used to compare the critical wind speed and frequency for various bridge sections studied in the literature (Morgenthal, 2002). The instability is conventionally evaluated based on the flutter derivatives, which are closely related to the system damping. The flutter derivatives can be estimated by forced vibration simulation.

Assuming that the periodic deflection and rotation with frequency ω cause the motion induced forces with the same frequency ω but with phase shift angle φ, Eqn. (1) and (2) can be combined with the forcing terms (Eqs. (3) and (4)) and rearranged as follows (Larsen and Walther, 1998):

$$C_L e^{i(\omega t - \varphi)} = 2K^2 \left[(iH_1^* + H_4^*) \frac{h}{B} + (iH_2^* + H_3^*)\alpha \right] e^{i\omega t} \tag{9}$$

$$C_M e^{i(\omega t - \varphi)} = 2K^2 \left[(iA_1^* + A_4^*) \frac{h}{B} + (iA_2^* + A_3^*)\alpha \right] e^{i\omega t} \tag{10}$$

where C_L and C_M are, respectively, the lift and moment coefficients representing the ratios of the lift force and moment to the wind flow force acting on the section. The flutter derivatives can be found based on the measured amplitude of the coefficients C_L and C_M, and the phase difference φ between the imposed periodic motion and the force coefficients as in Eqs. (9) and (10). Inserting the force terms (Eqs. (3) and (4)) expressed in terms of the flutter derivatives into the motion equations (Eqs. (1) and (2)) leads to a system dynamic equation.
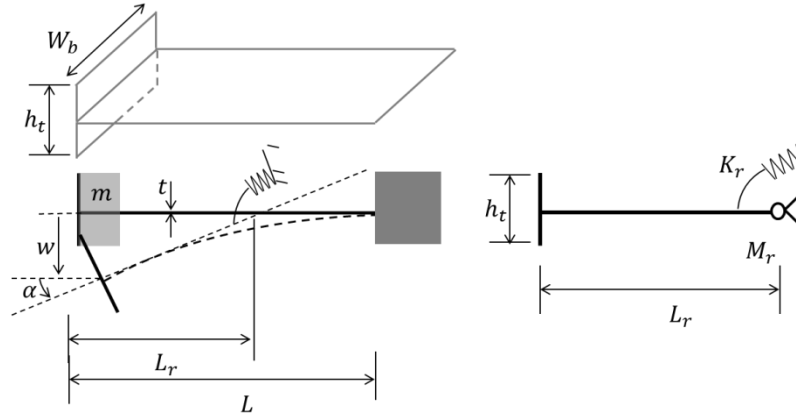
The eigenvalues of the derived system dynamic equation depict the characteristics of structural responses corresponding to wind induced forces. That is, when the real part of the complex eigenvalues of the system is negative, the system becomes unstable with excessive vibrational responses (Morgenthal, 2000). As to be discussed in the next section, we only consider the torsional mode of the T-shape cantilever energy harvester by treating the cantilever beam as a rigid body (1-DOF in rotation). In this case, the stability of the cantilever section can be evaluated by only considering the sign of the coefficient $\dot{\alpha}$ (angular velocity) in Eq. (5), which represents the system damping term. The negative system damping would indicate that energy is input into the system, which leads to exponentially increasing responses.

3. NUMERICAL FLUTTER SIMULATION

The flutter critical wind speed, at which flutter is initiated, the oscillating frequency, and the maximum tip displacement of the cantilever in the flutter based energy harvester are essential information for estimating the power output from the harvester. Due to the complexities inherent in the fluid structure interactions, the flutter information is almost impossible to calculate analytically. In this study, we use CFD simulations to compute the vibrational responses of the T-shape cantilever in the flutter based energy harvester. In addition, the flutter derivatives at different wind speeds are estimated to find the flutter critical wind speed. In this section, we only consider the mechanical intrinsic damping in the numerical simulation. The influence of the electromagnetic transducer, which imposes an additional electrical damping to the system, on the response will be considered in a later part of this paper.

3.1 Descriptions for the energy harvester model

The configurations and the mechanical parameters for the flutter based energy harvester section are depicted in Figure 3. The T-shaped cantilever, which is shown in Figure 3(a), is used to induce the large vortex induced force and, therefore, to initiate flutter at low wind speed. It should be noted that the geometry resembles that of a half H, which is well known as a sectional shape critical to torsional flutter through the Tacoma Narrows Bridge failure (Scott, 2001).

(a) Section dimension (b) Rigid body beam approximation

Figure 3: Flutter based energy harvester section and its rigid body beam approximation for CFD simulation.

Table 1: Parameters for the energy harvester

Model dimensions	Rotational mode
W_b (width) = 0.03 m	L_r (reduced length) = 0.0280 m
L (length) = 0.042 m	M_r (rotational mass) = $2.35 \cdot 10^{-4}$ Kgm^2
h_t (tip height) = 0.02 m	K_r (torsional stiffness) = 0.499 N
t (thickness) = $1.016 \cdot 10^{-4}$ m	ω_r (rotational frequency) = 46.1 rad/sec
m (mass) = 0.009 kg	
E (Elastic modulus) = 180GPa	
I (moment of inertia) = $2.62 \cdot 10^{-15}$ m^4	
K (stiffness) = 19.1103 N/m	
ω (natural frequency) = 46.1 rad/sec	
ζ_m (damping ratio) = 0.0040	

The CFD code allows a two-dimensional analysis where the solid sections remain rigid and can exert translational and rotational movements. It is therefore necessary to approximate the deflection of the cantilever in terms of the rotational motion of an equivalent rigid beam. To this end, a spring-supported rigid body is derived by seeking the equivalent rotational stiffness, the rotational mass and the reduced length as shown in Figure 3(b). The vertical deflection and the rotation under a unit force F exerting on the cantilever tip are calculated, respectively, as $w = FL^3/3EI$ and $\alpha = FL^2/2EI$. The length L_r of the rigid body section with the same rotation α can be approximated using the linear relationship $L_r\alpha = w$,

which results in $L_r = 2/3L$, where L is the length of the cantilever beam. The corresponding

rotational stiffness is then given as $K_r = FL_r/\alpha = 4EI/3L$. Furthermore, the rotational mass

(the moment of inertia) is computed as $M_r = mL_r^2 = 4mL^2/9$. The parameters for the original

cantilever section and the equivalent rigid frame are summarized in Table 1.

3.2 Forced vibration

The sign change in the A_2^* derivative can be used to identify the stability of the section and

torsional flutter of the SDOF system [16]. The A_2^* flutter derivative is determined using

forced vibration simulations at different wind speeds. The results are illustrated in Figure 4.

The A_2^* flutter derivative generally increases with the free stream wind speed, meaning that

the system becomes increasingly less stable at higher wind speed. For the cantilever energy

harvester model described in Figure 3 and Table 1, the A_2^* flutter derivative transits from the

negative value into the positive value around $U_\infty = 4.5 \sim 5.0$ m/s, which represents the flutter

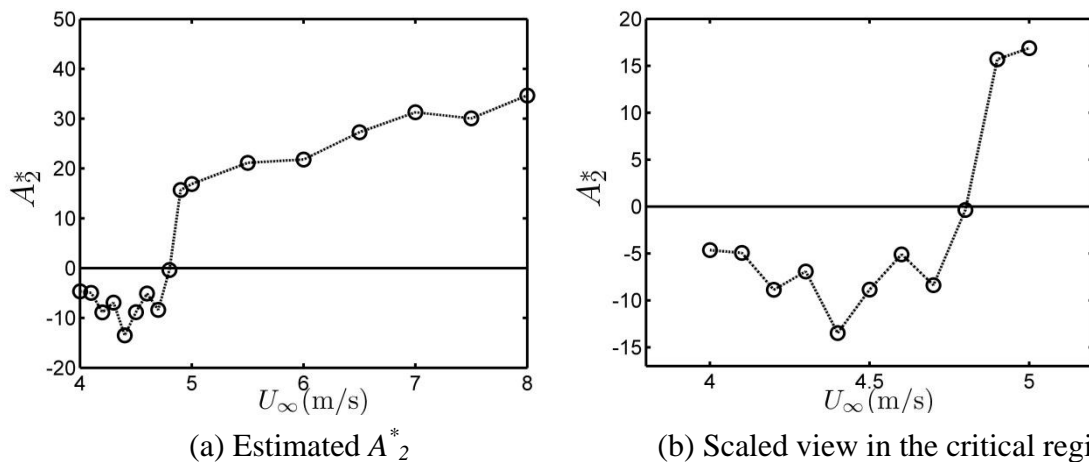critical wind speed separating the stable and unstable regions of the system response.

(a) Estimated A_2^* (b) Scaled view in the critical region

Figure 4: A_2^* flutter derivatives obtained from CFD simulation for the cantilever section whose parameters are described in Table 1.

3.3 Numerical fluid interaction analyses

The responses of the flutter based energy harvester are simulated by fully coupled fluid structure interaction simulations. Figure 5 shows a snap-shot of the T-shaped cantilever vibration showing the equivalent rigid frame model. Figure 6 shows the cantilever tip displacement time series corresponding to the wind speeds of 3 m/s and 4 m/s, respectively, which are lower and higher than the critical wind speed ($\approx$ 4.8 m/s). As shown in Figure 6 (b), when the wind speed is above the flutter critical wind speed, the amplitude of the tip displacement keeps increasing. The exponentially growing trend in the displacement is due to the negative damping in the system induced by the self exciting aerodynamic forces. Upon reaching an amplitude limit, the oscillation is bounded due to nonlinear aerodynamic effects at very large oscillation amplitudes.

For validation, the prototype harvester section whose dimensions are the same with the numerical simulation is made and tested in the laboratory. The result shows that the section starts to vibrate at the wind speed near 4~5 m/s, which is close to the estimated flutter onset speed by the numerical simulation.
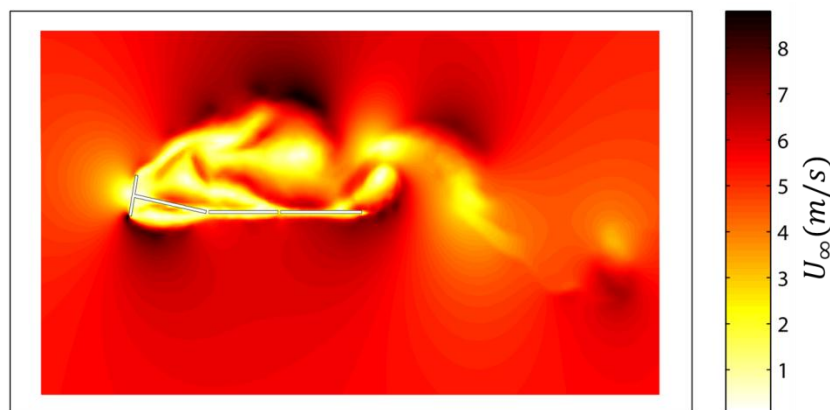

Figure 5: Fluid-structure interaction simulation for the cantilever section described in Table 1. The color represents wind speed (with 5.5 m/s wind speed)
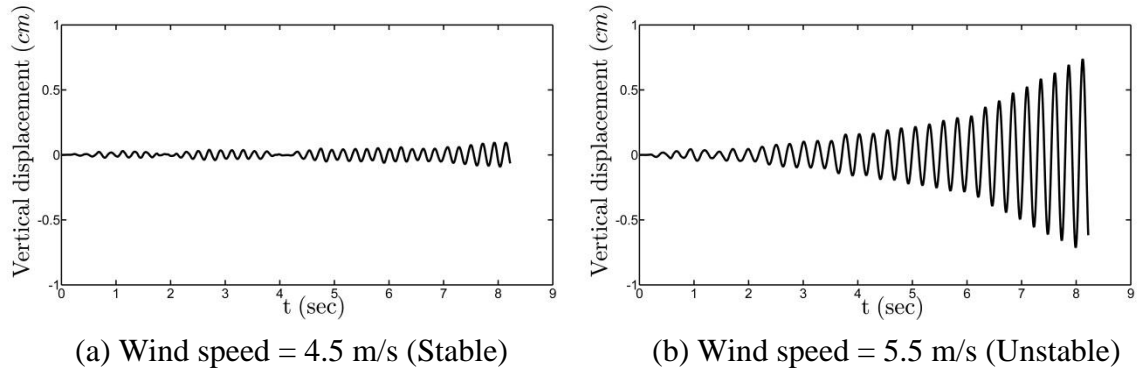
(a) Wind speed = 4.5 m/s (Stable)   (b) Wind speed = 5.5 m/s (Unstable)

Figure 6: Simulated tip displacement time series of the cantilever corresponding to different wind speeds using a CFD code, VXflow.

4. WIND TUNNEL EXPERIMENTS

The flutter based energy harvester includes three damping mechanisms: mechanical damping, electrical damping and aerodynamic damping. The mechanical damping dissipates mechanical energy of the vibrating cantilever, and the electrical damping extracts energy from the system and converts it into electrical energy. The aerodynamic damping either extracts energy from the system or inputs energy into the system depending on the wind speed (energy is infused into the system when the wind speed exceeds the flutter critical speed). The three damping mechanisms determine the vibrational motion of the flutter based energy harvester. In particular, the structural stability of the cantilever is determined by the relative magnitudes among the three damping coefficients. This section describes how to estimate the flutter onset wind speed based on the relationship among the three damping coefficients. In succeeding, the characteristics of the power output and the method for selecting the optimum load resistance in the energy harvester are discussed.

4.1 Wind tunnel experiment setup

Figure 7 shows the wind tunnel experimental setup. For the energy harvesting device, magnets are attached to the tip of the cantilever; the interaction between the magnets and the coils, which are attached to the inertial frame, induces the inductive voltage in the energy

harvester. The dimensions of the harvester section and the converted dimensions for the rigid body beam approximate model are the same with the previous numerical model. The attached coils have the 103 Ω of the coil resistance R_C and 2,800 of coil turns N.
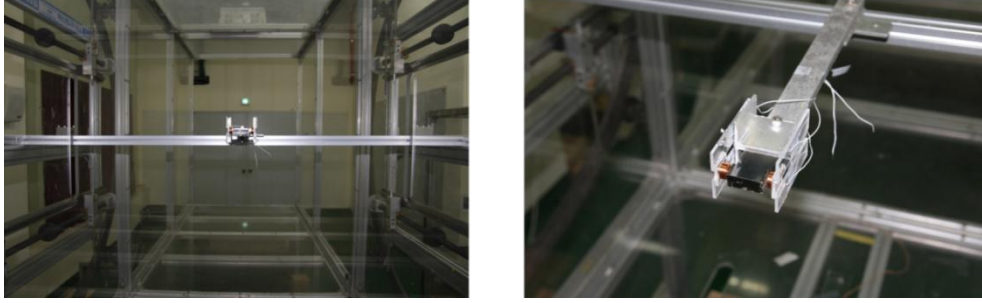

Figure 7: Wind tunnel experiment setting. Prototype energy harvester is placed inside of the wind tunnel. (KOCED Wind Tunnel Center, Chonbuk National University, Chonju, Korea)
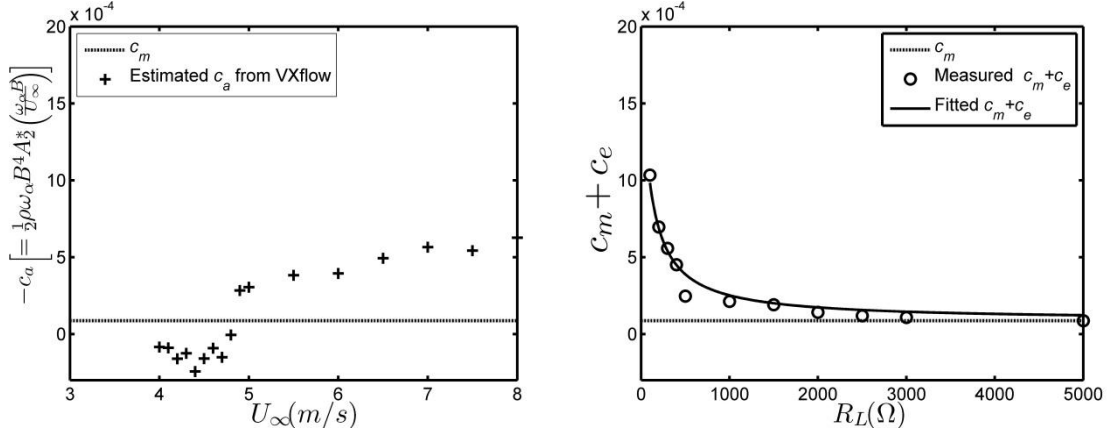
4.2 Prediction of flutter onset speed based on the three damping coefficients

Frist, the aerodynamic damping coefficients are calculated from the A_2^* flutter derivative obtained by the CFD forced vibration simulations with different wind speeds as illustrated in the previous section. The aerodynamic damping coefficient c_a is calculated as:

$$c_a = -1/2\,\rho U_\infty B^3 K A_2^*(K) = -1/2\,\rho B^4 \omega_\alpha A_2^*\left(\frac{B\omega_\alpha}{U_\infty}\right) \tag{11}$$

where ρ is air density. The reduced length L_r in Figure 3(b) is used for the section length B in Eq. (11). As seen in Eq. (11) the aerodynamic damping c_a is negatively proportional to the A_2^* flutter derivative (A_2^* increases with wind speed). The aerodynamic damping decreases as the wind speed increases, meaning that the section becomes increasingly less stable. The calculated aerodynamic damping coefficients at the different wind speeds are shown in Figure 8(a). Note that the negative aerodynamic damping coefficient $-c_a$ is plotted to easily

compare the relative magnitude between the aerodynamic damping and the sum of the mechanical and the electrical damping.

(a) Aerodynamic damping (b) Sum of mechanical and electrical damping

Figure 8: Comparison of aerodynamic damping and harvester damping for the prototype cantilever section: (a) the negative aerodynamic damping $-c_a$ estimated from the CFD simulations at different wind speeds (electrical transducer is not considered); (b) the calculated harvester damping coefficients determined using free vibration tests (no wind flow).

Second, free vibration tests are conducted to estimate the damping ratios (i.e., mechanical and electrical damping $c_m + c_e$) of the energy harvester, which are then converted into the mechanical damping and electrical damping coefficients. In the tests, the voltage time series generated by the interaction between the coils and the magnet is recorded. Then, the damping ratio is estimated form the exponential decaying rates of the amplitude peaks in the time series.

By changing the load resistance R_L from 100 Ω to 5000Ω, the electric damping coefficient c_e are calculated from the measured damping ratio ($c_e = 2\zeta_e M_\alpha \omega_\alpha$). In Figure 8b, the calculated c_e are represented with the red circles, from which the empirical models for c_e (Eq. (7)) is fitted. Note that the term $N\beta l$ in Eq. (7) can be found by measuring each of the terms, N, β and l. Measuring β, however, requires complicated magnetic flux analysis. As shown in Figure 8(b), the electrical damping coefficients follow the trend in the empirical

model of c_e. As the load resistance R_L increases, In addition, the sum of the electrical and the mechanical damping approaches to the structural damping represented by the dotted constant-level line since the electrical damping is inversely proportional to the load resistance R_L as seen in Eq. (7).

The stability of the energy harvester section can be evaluated on the basis of the separately calculated aerodynamic damping c_e and the harvester damping $c_m + c_e$. Assuming that the electrical damping can be linearly superimposed on the structural damping, the total system damping can be represented as:

$$c_m + c_e(R_L) + c_a(U_\infty) = 2M_\alpha \{\zeta_m + \zeta_e(R_L)\}\omega_\alpha - \frac{1}{2}\rho\omega_\alpha B^4 A_2^* \left(\frac{\omega_\alpha B}{U_\infty}\right) \qquad (12)$$

where $c_e = 2M_\alpha \zeta_e(R_L)\omega_\alpha$ is the added electrical damping coefficient. It can be seen from Eq. (12) that the system would become unstable and flutter would start when the total system damping $c_m + c_e + c_a$ becomes negative. In other words, when the negative aerodynamic damping $-c_a$ exceeds the sum of the electrical and the mechanical damping (i.e., $c_m + c_e(R_L) \le -c_a(U_\infty)$), the harvester starts producing electrical power.

The negative aerodynamic damping $-c_a$, which is a function of wind speed U_∞, and the sum of the mechanical and the electrical damping $c_m + c_e$, which is a function of the load resistance R_L, are compared in Figure 8. The term of $-c_a$ increases with wind speed (aerodynamic damping c_a decreases with wind speed), as shown in Figure 8(a). In contrast, the sum of the mechanical and the electrical damping decreases with load resistance R_L as shown in Figure 8(b). This is because the mechanical damping coefficient is constant, and the electrical damping coefficient is a decreasing function of load resistance. Therefore, the

flutter onset speed U_∞ can be found when $c_m + c_e = -c_a(U_\infty)$ for a given R_L. Similarly, when U_∞ is fixed the flutter onset resistance R_L can be found such that $c_m + c_e(R_L) = -c_a$.

When the electromagnetic transducer is open ($R_L = \infty$), the harvester damping $c_m + c_e$ is equal to the mechanical damping c_m. As shown in Figure 8, the mechanical damping is overcome by the aerodynamic damping at the wind speed between 4 m/s and 5 m/s. Both the experimental tests and the numerical simulations (as shown in Figure 4(b)) show that flutter starts at this estimated wind speed range. If the electromagnetic transducer is connected ($R_L < \infty$), the flutter onset speed increases due to the increased harvester damping $c_m + c_e$.

4.4 Energy outputs

The energy available from the flutter based energy harvester depends on the wind speed. Furthermore, the extractable energy is determined by the load resistance R_L. The influences of the wind speed and the load resistance on the RMS voltage and the RMS power are shown in Figure 9. In general, it can be observed that the levels of the RMS voltage and the RMS power increase with wind speeds. It can be seen in Figures 9(a) and 9(b) that both the voltage and the power outputs sharply increase at the wind speed between 4 ~ 5 m/s. This discontinuous trend is manifested particularly when the load resistance is 5000 Ω where the harvester damping approaches the structural damping. The measured flutter onset speed matches closely to the flutter onset speed estimated by the CFD simulation that does not include the electrical damping.
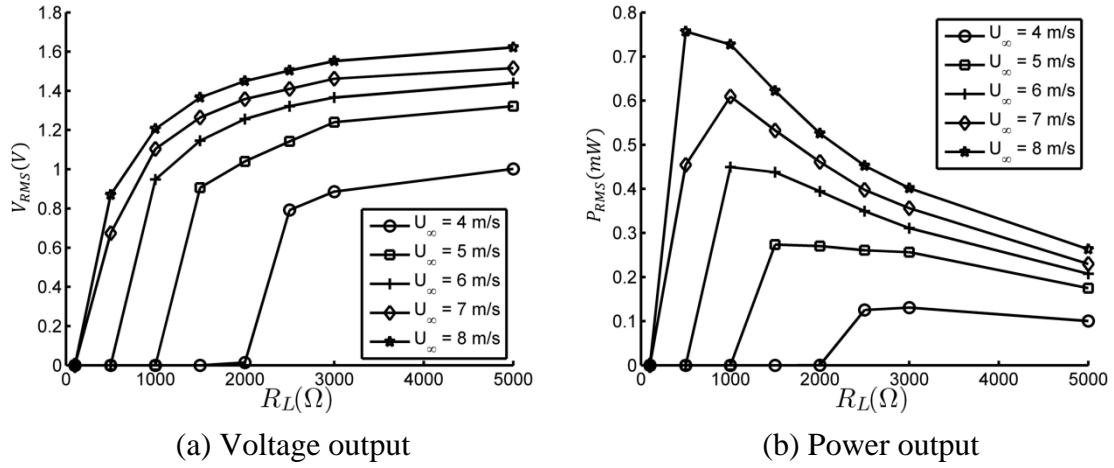
(a) Voltage output   (b) Power output

Figure 9: Measured outputs from the prototype energy harvester: (a) the root mean square voltages are calculated form a 30-sec time series for different wind speeds (4~8 m/s) and the load resistances R_L (100 ~ 5000 Ω); (b) the power outputs are calculated using the measured voltage time series for different wind speeds and the load resistance R_L.

As shown in Figure 9, the voltage outputs generally increase with the load resistance R_L. The power outputs, however, reach its maximum at a certain R_L and decreases as R_L further increases. These output trends are typical for energy harvesters with an electromagnetic transducer. It can also be observed that there exist noticeable discontinuous points in the voltage and the power curves in Figure 9, as the energy harvester produces energy only when the load resistance is larger than the flutter onset resistance. The critical load resistance is affected by the wind speed; as wind speed increases the flutter onset load resistance decreases. The discontinuous power curve is one unique feature of a flutter based energy harvester.

5. DISCUSSION

When designing an electromagnetic harvester using flutter as an input source, the optimum load resistance should be carefully chosen by taking consideration of the starting point of flutter as well as the level of power output and the wind speed distribution. The initiation of the flutter is determined by the relative magnitudes between the harvester damping and the

aerodynamic damping. The higher load resistance R_L is advantageous for initiating flutter on the harvester section. However, the corresponding power with the higher R_L is usually low due to the reduced electrical damping. The produced power is equivalent to the extracted energy from the vibrating section through the electrical damping as seen in Eq. (3). The variability of wind speed adds another complexity in the load resistance selecting procedure. As seen in the Figure 10, the wind speed is a random variable following a certain probability distribution $f_{U_\infty}(u)$. If the flutter based harvester is installed in the region where the mean wind speed is high, a low load resistance value that induces higher power can be selected.
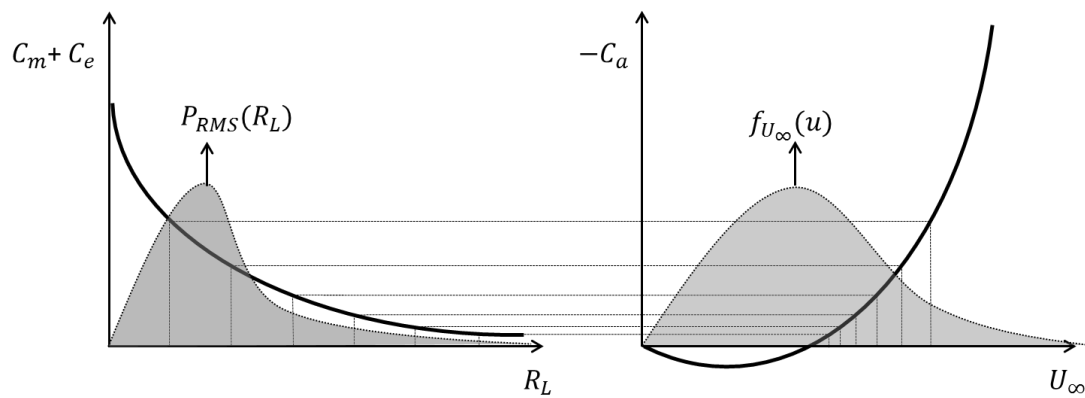

Figure 10: Factors for selecting the load resistance. The electrical and mechanical components determine the harvester damping curve, while the geometries of the section and mechanical parameters determine the aerodynamic damping curve. Wind speed is random variable.

Figure 11 shows a comparison between the measured and the calculated flutter onset load resistance. The flutter onset resistances are roughly measured by observing the voltage and power curves in Figure 9 The load resistance where the voltage or the power abruptly jumps from zero is assumed to be the flutter onset resistance. The measured values are then compared with the calculated values on the basis of two damping coefficient curves in Figure 8 and the criterion for the flutter onset ($c_m + c_e(R_L) \le -c_a(U_\infty)$). The comparison results are summarized in Figure 11. Note that the measured load resistance is represented by the range bar due to the coarse resolution in the load resistance variation during the tests. The onset

resistance generally decreases with wind speed because a higher wind speed can overcome larger amounts of electrical damping (small resistance corresponds to the large electrical damping). In general, the estimation based on the damping comparison underestimates the flutter onset resistance. However, the general trend is well captured by this approach which gives us insights into how to choose the optimal load resistance in a flutter based electromagnetic energy harvester.
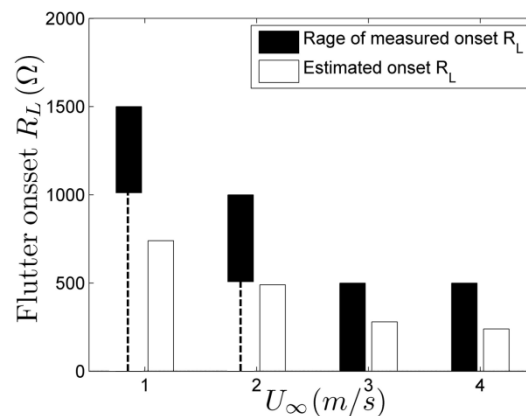

Figure 11: Comparison of flutter onset resistance: The measured R_L is found by observing the voltage and power outputs, while the calculated R_L is based on the damping comparison (R_L such that $\boldsymbol{c_m} + \boldsymbol{c_e}(\boldsymbol{R_L}) = -\boldsymbol{c_e}(\boldsymbol{U_\infty})$).

6. SUMMARY

This paper describes how numerical fluid dynamic simulations can be used to determine the flutter onset wind speed and the flutter onset load resistance of an electromagnetic energy-extracting harvesting device. The aerodynamic damping effect is determined from the flutter derivatives analysed using forced vibration simulations. Flutter begins when the negative aerodynamic damping coefficient exceeds the sum of mechanical and electrical damping. Below the critical wind speed the fluid extracts energy from the system and above that it feeds energy into the system. This fed energy is then converted into electrical power through the interaction between a magnet and a coil.

The CFD analysis for estimating the aerodynamic damping provides valuable insight into how to estimate the flutter onset speed and how to determine the load resistance, which is one of the important design parameters in the electromagnetic energy harvester. The load resistance affects the flutter onset wind speed and, at the same time, determines the level of power output by changing the electrical damping. Therefore, the optimum resistance should be selected to account for both the initiation of the flutter and the level of output power. The rigid body model in the numerical simulations appears to approximate the flutter induced cantilever vibration well in a linear region. The flutter onset speeds and the minimum load resistance estimated from the CFD analysis show similar tendency with the values measured from wind tunnel tests. CFD simulations can potentially be used to optimise the geometry of the wind induced energy harvester. In future work, the CFD model can be extended to take into consideration beam bending in order to estimate the system response more accurately.

REFERENCES

Roundy, S. and Wright, P.K. 2004. "A piezoelectric vibration based generator for wireless electronics," Smart Materials and Structures, 13:1131-1142.

Allen, J.J. and Smits, A.J. 2001. "Energy harvesting eel," Journal of Fluids and Structures, 15: 629-640.

Sun, C. et al. 2011. "PVDF microbelts for harvesting energy from respiration," Energy and Environmental Science, 4:4508-4512.

Jung, H., Kim, I. and Jang, S. 2011. "An energy harvesting system using the wind-induced vibration of a stay cable for powering a wireless sensor node," Smart Materials and Structures, 20, 075001.

Kwon, S. 2010. "A T-shaped piezoelectric cantilever for fluid energy harvesting," Applied Physics Letters, 97(16), http://dx.doi.org/10.1063/1.3503609.

Bryant, M., Wolff, E. and Garcia, E. 2011. "Aeroelastic flutter energy harvester design: the sensitivity of the driving instability to system parameters," Smart Materials and Structures, 20, 125017, doi:10.1088/0964-1726/20/12/125017.

Li, S., Yuan, J. and Lipson, H. 2011. "Ambient wind energy harvesting using cross-flow fluttering," Journal of Applied Physics, 109, http://dx.doi.org/10.1063/1.3525045.

Morgenthal et al. "Parallels between the wind excitation and the crowd loading of bridges,"

Larsen, A. 1998, "Advanced in aeroelastic analyses of suspension and cable-stayed bridges," Journal of Wind Engineering and Industrial Aerodynamics, 74-76, 73-90.

Morgenthal, M. 2007. "An Immersed Interface Method for the Vortex-in-Cell Algorithm," Computers and Structures, 85: 712-726.

Scanlan, R.H. and Tomko, J.J. 1971. "Airfoil and bridge deck flutter derivatives," Journal of Engineering Mechanics, 97: 1717-1737

Theodorsen, T. 1935. "General theory of aerodynamic instability and the mechanism of flutter," NACA Report 496.

Beeby, S.P. et al. 2007. "A mirco electromagnetic generator for vibration energy harvesting," Journal of Micromechanics and Microengineering, 17: 1257-1265.

El-hami, M. et al. 2001, "Design and fabrication of a new vibration-based electromechanical power generator," Sensors and Actuators A: Physical, 92: 335–342.

Larsen, A. and Walther, J.H. 1998. "Discrete vortex simulation of flow around five generic bridge deck sections," Journal of Wind Engineering and Industrial Aerodynamics, 77&78: 591-602.

Morgenthal, G. 2002, "Aerodynamic Analysis of Structures Using High-resolution Vortex

Particle Methods," Ph.D Thesis, University of Cambridge, UK.

Morgenthal, G. 2000. "Fluid-Structure Interaction in Bluff-Body Aerodynamics and Long Span Bridge Design: Phenomena and Methods," Tech. Rep. CUED/D-STRUCT/TR.187, University of Cambridge, UK.

Scott, R. 2001. "In the Wake of Tacoma," ASCE, Reston.